Effect of Vibration on Agglomerate Particulate Fluidization

Jose Manuel Valverde and Antonio Castellanos
Faculty of Physics. Universidad de Sevilla, Avenida Reina Mercedes s/n, 41012 Sevilla, Spain

DOI 10.1002/aic.10769
Published online February 10, 2006 in Wiley InterScience (www.interscience.wiley.com).

Agglomerate particulate fluidization (APF), consisting of uniform bubbleless fluidization of agglomerated fine particles, has been observed in some fluidized beds of fine and ultrafine powders. Experiments performed in centrifugal fluidized beds (CFB) and vibrofluidized beds (VFB) show that the quality of fluidization is improved by increased effective acceleration. The Richardson-Zaki modified equation is used, and a proposed criterion for agglomerate size is presented in order to predict the effect of the increase of gravitational acceleration on the APF bed. Following, model predictions are compared with experimental data on VFB of xerographic toners (particle size $\approx 10\mu$ *m) displaying APF in a wide interval of gas velocities. It is seen that the agglomerate size and agglomerate volume fraction* ϕ^* *decrease as the effective acceleration is increased. The agreement with the model predictions is good, but at some critical acceleration visible bubbling is stimulated. At bubbling stimulation* ϕ^* *is close to the value of* ϕ^* *at the onset of bubbling in the absence of external vibrations when the gas velocity is increased up to the minimum bubbling velocity. This result indicates that the agglomerate size cannot be decreased indefinitely since at some critical point the concentration and size of local voids can be higher enough to yield the irreversible coalescence of voids into large bubbles. Particle agglomeration is, therefore, essential at some extent to the uniform fluidized state observed for fine particles.* © 2006 American Institute of Chemical Engineers *AIChE J,* 52: 1705-1714, 2006
Keywords: fluidization, particle technology

Introduction

Gas-fluidization of fine particles (particle size $d_p <\approx 20$ μ m) is being the subject of extensive research partly due to its potential for the improvement of gas-solid reaction efficiency. This is especially true in the case of nanoparticles.[1-10] For example, fluidized beds of TiO_2 nanoparticles have been proposed to treat air pollutant nitrogen oxides by photocatalytic reaction, which is accelerated in the fluidized bed, because of the large specific surface area.[1] However, and due to the exceedingly large ratio of interparticle attractive force to particle weight, fine and ultrafine particles agglomerate in the fluidized state. Primary particle size and density cannot be, therefore, used as the parameters for predicting the fluidization behavior of fine and ultrafine particles. On the other hand, and since fluidized agglomerates are formed dynamically in the fluidized bed, it is difficult to measure experimentally their properties. *In situ* images of fluidized agglomerates have been obtained with the aid of a laser source focused on the fluidized bed surface,[4,8] but this technique can only be applied to observe superficial agglomerates and cannot give information on the agglomerate density or, equivalently, its fractal structure. SEM analysis has been applied to agglomerates acquired directly from the fluidized bed by adhesive tape[3] or aspiration.[4] In a previous report we visualized fine particle agglomerates extracted from the fluidized bed by adhesion to a sheet of paper.[11] These techniques have the main inconvenience that intrusiveness might affect agglomerate properties in the extraction pro-

Correspondence concerning this article should be addressed to J-M. Valverde at jmillan@us.es.

cess. X-ray imaging is being currently developed to allow fluidized beds to be studied at length scales down to 400 nm and temporal resolutions of 1ms, with the advantage of studying the bulk of the fluidized bed in a nondestructive and dynamic manner.[12] However, the technique needs further development in order to respond to the low X-ray energies required for some fine powder samples.[12] A parallel effort is, thus, needed in the formulation of models that predict agglomerate relevant parameters, such as size and density from the basis of a clear physical understanding of particle agglomeration dynamics. The effect of acting forces, such as interparticle attraction, gravity and gas flow shear forces, and other parameters such as gas viscosity needs to be further rationalized.

Two distinct behaviors are generally found in gas-fluidized beds of fine and ultrafine particles. In some cases smooth fluidization occurs with extremely high-bed expansion and absence of visible bubbles in a wide interval of gas velocities.[8,13,14] This kind of fluidization is so called agglomerate particulate fluidization (APF). For other cases heterogeneous fluidization is observed with limited bed expansion and large visible bubbles.[8] This type of fluidization has been called agglomerate bubbling fluidization (ABF). In the APF state, the bed expands uniformly according to the modified Richardson-Zaki equation[11] since the superficial gas velocity is similar to the initial settling velocity v_s in sedimentation[15]

$$\frac{v_g}{v^*} \simeq \frac{v_s}{v^*} = (1 - \phi_0^*)^n \tag{1}$$

where $v^* = v_{p0}N_0/k_0$ is the settling velocity of a single agglomerate, $\phi_0^* = \phi_0 k_0^3/N_0$ is the volume fraction of the agglomerates, and $n \approx 5$ is an empirical parameter; ϕ_0 is the particle volume fraction, N_0 is the number of particles in the agglomerate, k_0 is the ratio of agglomerate size to particle size (related to N_0 by the fractal dimension of the agglomerate $D = \log N_0 / \log k_0$), and v_{p0} is the Stokes settling velocity of a single particle

$$v_{p0} = \frac{1}{18}\frac{(\rho_p - \rho_f)\, g_0 d_p^2}{\mu} \tag{2}$$

where ρ_p is the particle density, ρ_f is the gas density, $g_0 = 9.81$ m/s^2 is the gravity field, and μ is the viscosity of the gas. According to the theoretical derivation by Batchelor et al.[16] $n = 5.6$ for fluidized beds in the dilute limit and operated in the small Reynolds number regime. Thus, Eq. 1 can be rewritten as

$$\frac{v_g}{v_{p0}} = k_0^{D-1}(1 - k_0^{3-D}\phi_0)^{5.6} \tag{3}$$

The fit of Eq. 3 to experimental data has been used to predict the size and fractal dimension of fluidized agglomerates.[4,11] From settling experiments, which consist of suddenly stopping the gas flow after the fluidized bed has reached a stationary condition while $v_s(\phi_0)$ is measured, we derived the power law $N_0 \sim Bo_{g0}^{\alpha}$ ($\alpha \simeq 0.7$).[11] Here (granular Bond number) Bo_{g0} is the ratio of interparticle attractive force in the fluidized bed to particle weight

$$Bo_{g0} = \frac{F_0}{m_p g_0} \tag{4}$$

being m_p the particle mass. The fractal dimension of the predicted agglomerates is a robust parameter of the fit around $D = 2.5$, in agreement with the diffusion-limited-agglomeration (DLA) model, based on particle-cluster aggregation mechanism. Equation 1 can be easily translated to nanoparticle APF,[17] where complex agglomerates are formed by a multistage process consisting of agglomeration of pre-existing simple agglomerates.[3] For ABF beds, v_g is appreciably larger than v_s since bubbles allow for a bypass of a substantial volume of gas,[18] thus, denying the applicability of Eq. 3.

Experimental studies on centrifugal fluidized beds (CFB) of nanoparticles indicate that the mean agglomerate size decreases as the centrifugal acceleration is increased, while at the same time bed expansion and uniformity of fluidization is improved.[6] Nam et al.[4] coupled aeration with vibration to achieve homogeneous smooth expansion of nanoparticle fluidized beds due to the breakup of large agglomerates. Using a high-speed laser imaging system, Hakim et al.[10] have shown that the size of fluidized agglomerates of nanoparticles is decreased as vibration frequency is increased. Agglomerate size reduction in vibrofluidized beds (VFB) of microsized particles has been also inferred from measurements of gas velocity and gas pressure drop.[19]

Both in CFB and VFB the decrease in the agglomerate mean size can be attributed to the increase of the separation effect of the gravitational acceleration in detriment of the cohesive effect of interparticle attraction. Semiempirical models have been reported to estimate the agglomerate size reduction in CFB[6] and VFB,[19] based either on force or on energy balance equations. Matsuda et al.[6] have proposed an energy balance equation, but their prediction relies on the assumption that there exists an attainable energy for disintegration of agglomerates E_a proportional to g_{ef}^n, where g_{ef} is the effective acceleration in the CFB and n is adjusted to 0.4 in order to fit the model prediction to their experimental results. Mawatari et al.[19] wrote a force balance between the cohesive force (van der Waals attractive force) and the separation forces (gravity, vibration, and shear force by the gas flow), in which the vibrational force is considered to act on the agglomerate by increasing the gravitational acceleration $g_{ef} \simeq g_0\Lambda$, where

$$\Lambda = 1 + \frac{A\omega^2}{g_0} \tag{5}$$

A is the vibration amplitude and $\omega = 2\pi f$, being f the vibration frequency. However, the empirical equation used for the shear force depends on the gas velocity and void fraction, and to estimate the agglomerate size they were forced to use particular data on the lower limit of gas velocity for channel breakage and the void fraction at this gas velocity. Fractal agglomerates screen the surrounding gas flow very effectively,[8] thus, preventing higher gas-solid contact and hampering reaction efficiency. The study of the effect of vibration on fluidized agglomerates may have therefore a relevant impact on industrial applications.

The *in situ* images of fluidized nanoparticle agglomerates

obtained by Hakim et al. offer evidence of dynamic aggregation behavior.[10] Essentially particle agglomeration results from a dynamic equilibrium between interparticle attractive force and flow shear that in the gravity field supports particles weight. In a recent article[20] we have proposed a scaling law to estimate the limit size of gas-fluidized particle agglomerates inspired in a previous study on the limits to gelation in the clustering of athermal colloidal particles.[21,22] In fact, from the gas frame of reference, APF beds can be considered as similar physical systems to settling suspensions of aggregated particles.[15] The hydrodynamic drag on the agglomerate, which acts mainly at its surface, balances the gravity force, which is a body force acting uniformly through the agglomerate. As a consequence shear forces appear distributed across the agglomerate that grow as the agglomerate size increases eventually curtailing its growth. The response of the agglomerate resembles that of a spring subjected to a typical strain[21]

$$\gamma \sim \frac{N_0 m_p g_0}{K_c R_c} \tag{6}$$

where K_c is the agglomerate spring constant and $R_c = k_0 d_p/2$ is the aggregate radius. K_c is given by ζ_0/k_0^{β}, being ζ_0 is the interparticle force constant, and the elasticity exponent $\beta = 3$ is in the 3-D case.[22] In order to find the agglomerate limit size in APF we estimated that the maximum shear force that the agglomerate can stand must be of order of the interparticle attractive force. From Eq. 6 the local shear force acting on the agglomerate is

$$F_s \sim \zeta_0 \gamma d_p/2 \sim m_p g N_0 k_0^2 \tag{7}$$

which leads to the simple criterion

$$Bo_{g0} \sim k_0^{D+2} \tag{8}$$

Equation 8 gives a maximum number of particles per agglomerate $N_0 = k_0^D \sim Bo_{g0}^{D/(D+2)} \simeq Bo_{g0}^{0.6}$ for DLA agglomerates (D = 2.5), in close agreement with our previous experimental results.[11] Although F_0 may increase by gas adsorption to the surface of the particles, this effect is negligible at ambient pressure.[23] Hence, Eq. 8 predicts that the agglomerate size should not depend essentially on the type of gas. Accordingly, we obtained in our experimental work using nitrogen or neon as fluidizing gases at ambient conditions,[24] that there is not a relevant distinction between the agglomerates fluidized with different gases. Again, Eq. 8 can be translated to nanoparticle APF assuming that the mechanism of aggregation of preexisting simple agglomerates into complex agglomerates is controlled by the same physical mechanism as for aggregation of fine micrometric particles.[17]

Effect of Effective Acceleration on Particle Agglomeration in the APF State

In this article we will look at the effect of varying the effective acceleration on particle agglomeration and bed expansion. For an APF bed subjected to an effective acceleration, at the stationary state the particle volume fraction will be ϕ, the number of particles per agglomerate will be N, and the relative size of the agglomerate k. We will assume that the fractal dimension of the agglomerates does not change, only their size. In the particular case of the VFB, the instantaneous acceleration is $g(t) = g_0 + a_c(t)$, where $a_c(t) = A\omega^2 \sin(\omega t)$, thus, the time average is $\langle g(t) \rangle = g_0$. This means that in the limit of an individual particle ($\phi \to 0$), it will settle as in the gravity field, that is, $v_p \approx v_{p0}$ in the R-Z equation. On the other hand, in the new dynamical process of agglomerate formation, agglomerates are eroded when $g(t) > g_0$. Conversely agglomerates should reform when $g(t) < g_0$, but this requires that the typical time t_p for an agglomerate to travel a distance of the order of its size should be smaller than the vibration semiperiod $T/2 = 1/(2f)$, during which $g(t) < g_0$. Since, $t_p \sim kd_p/v_f$, where $v_f \sim v_g$ [32] is the typical fluctuation velocity of the particles, and using $kd_p \sim 50$ μm and $v_g \sim 5$ mm/s as typical values,[18] we have $t_p \sim 0.01$ s.. Thus, for vibration frequencies $f > \approx 50$ Hz agglomerate reconstruction is not likely when $g(t) < g0$. Accordingly, Eqs. 3 and 8 should be rewritten as

$$\frac{v_g}{v_{p0}} = k^{D-1}(1 - k^{3-D}\phi)^{5.6} \tag{9}$$

$$Bo_g \sim k^{D+2}, \tag{10}$$

where

$$Bo_g = \frac{F_0}{m_p g_{ef}} \tag{11}$$

with $g_{ef} \sim g_0 \Lambda$ ($\Lambda = 1 + (A\omega^2/g_0)$).

Using Eqs. 4, 8, 10 and 11, we may predict the new agglomerate relative size

$$k \sim \frac{k_0}{\Lambda^{1/(D+2)}} \tag{12}$$

From Eqs. 3, 9, and 12, the particle volume fraction at the new effective acceleration should be

$$\phi \sim \frac{1 - \Lambda^{(D-1)/[5.6(D+2)]}(1 - k_0^{3-D}\phi_0)}{k_0^{3-D}/\Lambda^{(3-D)/(D+2)}} \tag{13}$$

A goal of this work is to check whether Eq. 13 predicts reasonably well experimental data on VFB of fine powders. Equation 13 is based on the assumption that the fractal dimension of the agglomerates does not change, which is reasonable since particles will be preferentially eroded from the external surface of the agglomerate by flow shear. Moreover, measurements on vibrofluidized beds[4] yield similar values of D (close to $D = 2.5$) as for nonvibrated APF beds.[8,11]

Experimental Setup

Our fluidized bed system has been extensively described in previous reports.[25-27] Parts of the experimental results shown in this study were previously reported in[27]. Figure 1 shows the experimental setup. The powder sample is held in either a 2.52 cm or 4.42 cm dia. cylinder made of polycarbonate (in this way

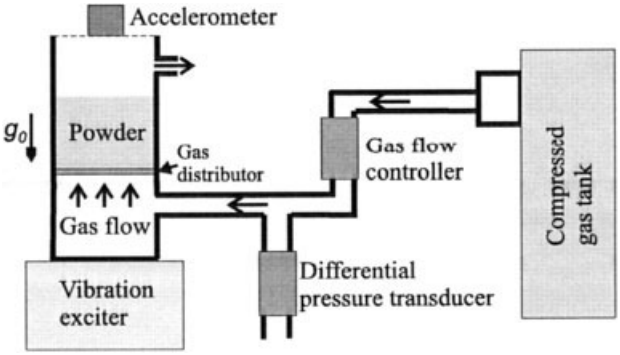

Figure 1. Experimental setup for vibrofluidized bed experiments.

wall effects are ruled out), the base of which is a sintered metal filter of 5 m pore size that acts as gas distributor. Dry nitrogen is supplied from a tank of compressed gas, and a gas flow controller is used to adjust the superficial gas velocity with a maximum accuracy of 0.01 mm/s. By using dry nitrogen we minimize the effect of moisture on the interparticle cohesion. Charge spectrograph measurements made at Xerox Co. indicate also that electrostatic forces are minimal as compared to van der Waals forces, which are, therefore, the main source of interparticle attraction. The average bed height was measured by a video camera coupled to a strobe light (2.52 cm dia. bed), or by an ultrasonic emitter-receiver (4.42 cm dia. bed) placed on top of the bed that determines distance accurately ($\Delta H \simeq \pm 0.01$ cm) by sending an ultrasonic wave and measuring the time of reflection from the bed free surface. From the fluidized-bed height H, and the particle density ρ_p, we compute the average particle volume fraction $\phi = m/(\rho_p SH)$, where m is the powder mass used (typically $m \approx 10$g), and S is the area of the gas distributor. In all the experiments the gas flow is set after the bed has been conveniently initialized in a bubbling state by previously imposing a large enough gas flow. In the bubbling regime the fluidized bed looses memory of its previous history,[28] thus, experimental results in the nonbubbling fluidized regime are reproducible. To test the behavior of the fluidized bed when subjected to vertical vibrations, it was mounted on an electromagnetic vibration exciter driven by a signal generator, which provided sinusoidal, vertical vibrations of controlled frequency f. The frequency of the oscillations could be controlled to within $\pm$ 0.1Hz in the range from 10 to 1,000 Hz. The amplitude of vibrations A was monitored using a piezoelectric accelerometer glued to the cylinder and varied in the range A $\approx$ (1,100) μ m, which was much smaller that the bed height H $\approx$ 1cm.

Experimental Powders

The powders used in the experimental measurements consist of xerographic toners, whose mechanical and fluidization properties have been explored in detail previously.[11,14,18,20,27,29,30-33] Typical toner particle size is of the order of 10 microns and the base material is polymer. In the manufacturing process, aerodynamic classification is employed in order to produce a narrow toner particle-size distribution. However, these particles are not perfectly smooth spheres, and the measured values of interparticle adhesion are very sensitive to surface asperities as a consequence of the short-range nature of van der Waals attractive forces.[30] To reduce the van der Waals force, hard nanoparticles are blended with toner particles in order to coat the toner particle surfaces so that the contacting surfaces become roughened. For the Xerox toners employed in this study Aerosil R812 7nm particles (hydrophobic fumed silica) are used in order to control flow properties as interparticle attractive force is decreased.[29] For the commercial Canon CLC700 toner the presence of titania nanoparticles has been detected by SEM analysis. Nevertheless, a main role of these hard nanoparticles is that they attenuate the rapid increase of the interparticle adhesion force with the load applied on the interparticle contact, and also with the time of application of the load, which is characteristic of plastic particles.[30] Thus, the addition of silica prevents hard caking and facilitates fluidization when use is resumed, preventing the common tendency of fine powders to cake when they are allowed to lie dormant for a long time between periods of use or they are subjected to very large loads.

The relevant physical properties for the powders employed in this investigation are summarized in Table 1. Figure 2(left) shows SEM pictures of Xerox and Canon toners, where it can be appreciated the angularly shaped profile of Canon toner particles in contrast with the rounded aspect of Xerox toner particles. Figure 2(right) shows photographs of Xerox toner particles taken from the fluidized bed (see ref. [11]). In the next Figure (Figure 3) we present a close view of Xerox toner particle surface showing a quite homogeneous distribution of the coating silica nanoparticles.

Nonvibrated fluidized-bed properties

A common characteristic for the fluidized xerographic toners is that they exhibit APF, that is, they can be uniformly fluidized, for an extended window of gas velocities due to the agglomeration of primary particles into porous light agglomerates. These agglomerates are highly effective in bubble splitting, thus, allowing the fluidized bed to achieve the condition of bubbleless fluidization.[24] The average agglomerate size and fractal dimension for the powders used in this study were measured from settling experiments.[11,18] Figure 4a shows data of the initial settling velocity of the top free surface v_s vs. the particle volume fraction ϕ of the fluidized bed. The experimental results can be well described by the modified R–Z equation (Eq. 3). The best fits of this equation to the data yield the values of k_0 and D given in Table 1. Figure 4b is a plot of

Table 1. d_p is Volume Average Particle Size, ρ_p is Particle Density, *SAC* Is Surface Additive Coverage, k_0 is the Ratio of Agglomerate Size in Fluidization to Particle Size, and D is the Fractal Dimension of the Agglomerates

Toner	Material	d_p (μm)	ρ_p (kg/m^3)	SAC	k_0 ($\pm\sim$0.4)	D ($\pm\sim$0.01)
RT5117-3 (Xerox)	Styrene-butadiene copolymer	12.7	1065	80	2.8	2.53
RT5116-3 (Xerox)	Styrene-butadiene copolymer	12.7	1065	40	3.2	2.51
CLC700 (Canon)	Polyester	8.5	1200	$\sim$100	5.7	2.61

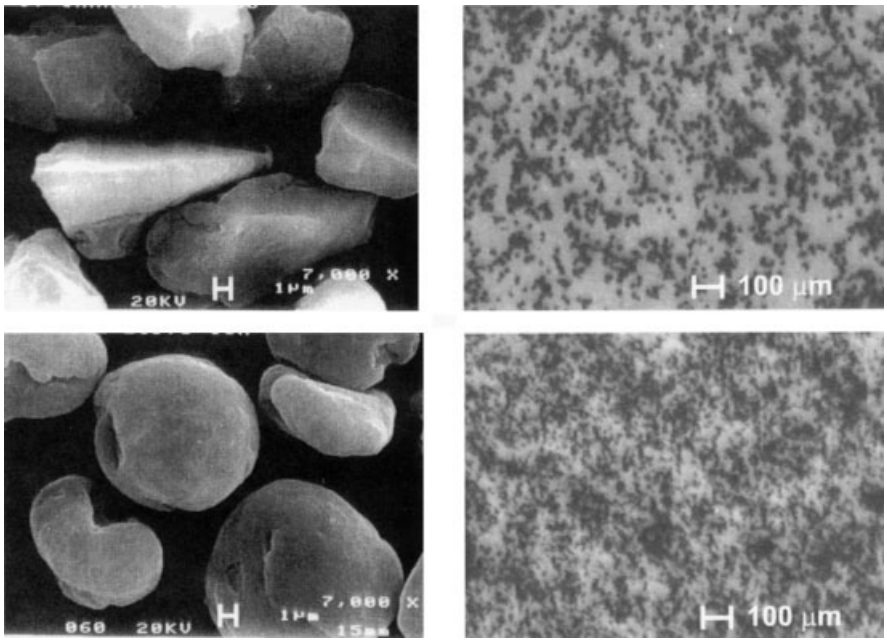

Figure 2. Left: Scanning Electron Microscope (SEM) pictures of Canon (top) and Xerox (bottom) toner particles; right: pictures obtained from the optical microscope of toner particle agglomerates taken from the fluidized bed according the process detailed in ref. [11] showing that the level of agglomeration increases as particle size is decreased (the top photograph corresponds to 19.1 μm primary particle size and the bottom one to 7.8 μm primary particle size).

ν_s vs. the superficial gas velocity in fluidization ν_g, showing that they are similar in the homogeneous fluidization window as it must be expected for APF. Contrarily, ν_s is clearly smaller than ν_g in the ABF regime since bubbles allow for a bypass of an appreciable volume of gas, thus, curtailing further expansion of the bed as can be seen in Figure 5, where we show data of ϕ vs. ν_g. It is clear from Figure 4a that the relative size of CLC700 agglomerates is larger than the relative size of Xerox toner agglomerates, that is, for a given ϕ the relative settling velocity is appreciably larger. This is due to the smaller primary particle size of CLC700 toner, and agrees with our previous result[11] expressed by Eq. 8. On the other hand, the relative size of agglomerates for Xerox toners are quite similar since both toners have similar Bond numbers.

In Figure 5 we have delineated the APF window for the CLC700 toner, which has been determined from a series of extensive measurements of the local concentration of solids and bed height fluctuations.[32] Fluidization is uniform (APF) for this toner in the window 0.3 cm/s $< v_g <$ 0.7 cm/s (this information will be relevant in our oncoming analysis of the vibrofluidized bed). For $v_g >$ 0.7 cm/s, macroscopic gas bubbles are developed, and the ABF regime begins although this transition is not sharply marked. Heterogeneous structures, such as channels and craters appear for $v_g <$ 0.3 cm/s, whereas for $v_g <$ 0.1 cm/s the bed enters a solidlike fluidized regime.[31] The initiation of the ABF regime is also indicated in Figure 5 for the Xerox toners. An important feature inferred from Figures 4b and 5 is that incipient bubbling is considerably delayed for the CLC700 toner. This is basically related to the larger relative size of their agglomerates in accordance with our previous result that the interval of APF increases as the granular Bond number increases.[14] The formation of large gas

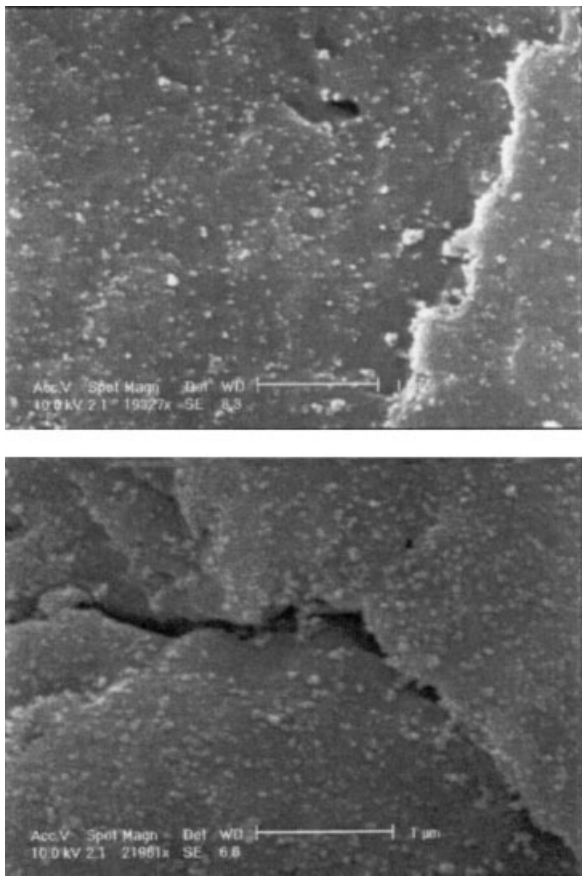

Figure 3. SEM pictures of toner particle surfaces with 32% (top) and 64% (bottom) of surface additive coverage (SAC).

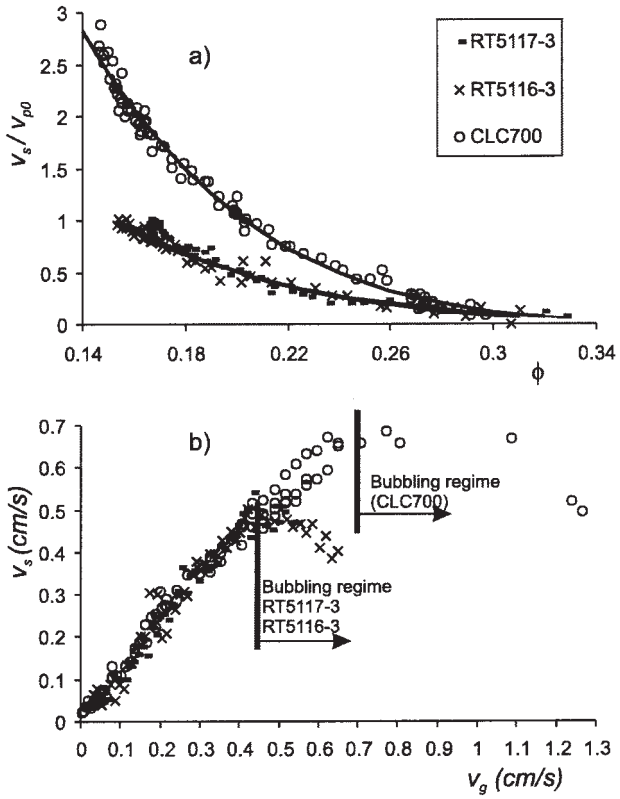

Figure 4. (a) Settling velocity of the top free surface of the fluidized bed (relative to the settling velocity of an individual particle) measured just after shutting off the gas supply vs. the particle volume fraction of the previously fluidized bed; the continuous lines are best fit curves from the modified R–Z equation (Eq. 3), and (b) Settling velocity vs. superficial gas velocity.

The onset of bubbling is delineated and coincides with the departure from the equation $v_s \sim v_g$ characteristic of APF.

pockets at the onset of bubbling can be understood as the result of the rapid coalescence of small voids that cannot be counterbalanced by void splitting mechanism when their concentration reaches a critical value.[24] According to the relative size k_0 and fractal dimension D derived for the agglomerates, we estimate that the agglomerate volume fraction ϕ^* at incipient bubbling is $\phi^*_{bub} = k_0^{3-D}\phi_b \simeq 0.3$ for CLC700 toner, is $\phi^*_{bub} \simeq 0.275$ for the RT5117-3 toner, and is $\phi^*_{bub} \simeq 0.266$ for the RT5116-3 toner. This is the minimum volume fraction of agglomerates that can be sustained from their hydrodynamic interaction with the gas.

Vibrated fluidized bed results

We have plotted in Figure 6 some examples of the evolution of the particle volume fraction of the fluidized powder ϕ, as the bed is vertically vibrated at fixed frequency when vibration amplitude is slowly increased. During the experiment the superficial gas velocity v_g is held constant, smaller than the minimum bubbling velocity ($v_g < v_b$), but large enough to drive the bed into APF in the initial state. First we observe a gradual expansion of the bed as predicted by the theoretical analysis, based on agglomerate size reduction due to increased effective acceleration $g_{ef} = g_0(1 + A\omega^2/g_0)$. At some critical acceleration g_c, there is, however, a clear departure from the expected trend, instead premature development of large bubbles is stimulated by vibration and, consequently, the bed height decreases markedly. As the acceleration is further increased, ϕ increases markedly as a consequence of the increase of the size of the stimulated gas bubbles. Before the stimulation of bubbling, the prediction of Eq. 13 is a good fit to the data within the experimental scatter of the values of k_0 and D previously determined from settling experiments[11,18] (Table 1). In Figure 6 we have plotted theoretical curves for several values of D. It can be seen that Eq. 13 is very sensitive to D. This sensitiveness arises from the strong dependence of the R–Z equation on D allowing us to have accurate values of D for our powders. It is worth noting that Eq. 13 would predict a collapse of the vibrofluidized bed (see Figure 6) rather than an expansion for systems of agglomerates formed by mechanisms of cluster-cluster aggregation, such as diffusion-limited colloidal aggregation (DLCA, $D \approx 1.8$) or reaction-limited colloidal aggregation (RLCA, $D \approx 2.1$) typically observed in colloidal suspensions.

Figure 7 shows the behavior at different frequencies. It can be said that, within the experimental scatter, the experimental curves have a common envelope that is well described by Eq. 13, whereas the critical acceleration for bubbling stimulation increases in general with the vibration frequency. In Figure 8 we show a close view to the minimum particle volume fraction ϕ_{min}, defined as the value of just before bubbling stimulation, as a function of g_c/g_0. We have also plotted in Figure 8 the curve predicted by Eq. 13. As can be observed the agreement of the predicted values with the experimental data is good within the experimental scatter.

The question pending is: why is bubbling stimulated at some point by vibration? Before analyzing in further detail this intriguing result, let us see the effect of vibration on the heterogeneously fluidized bed, which is characterized by the existence of channels and craters that cause a heterogeneous

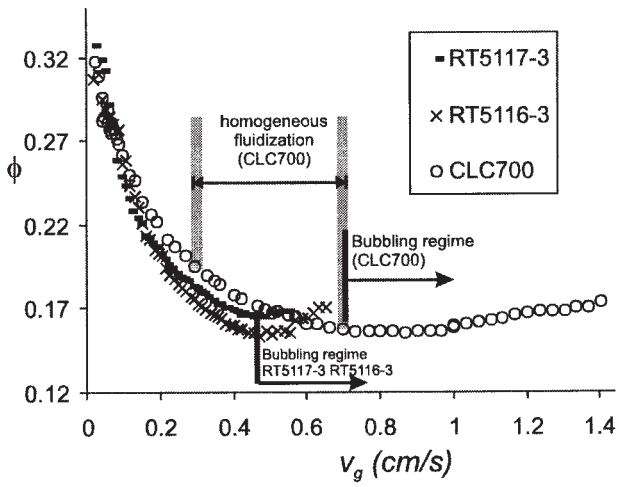

Figure 5. Particle volume fraction of the fluidized bed vs. gas velocity.

The interval of uniform fluidization is delineated for CLC700 toner.

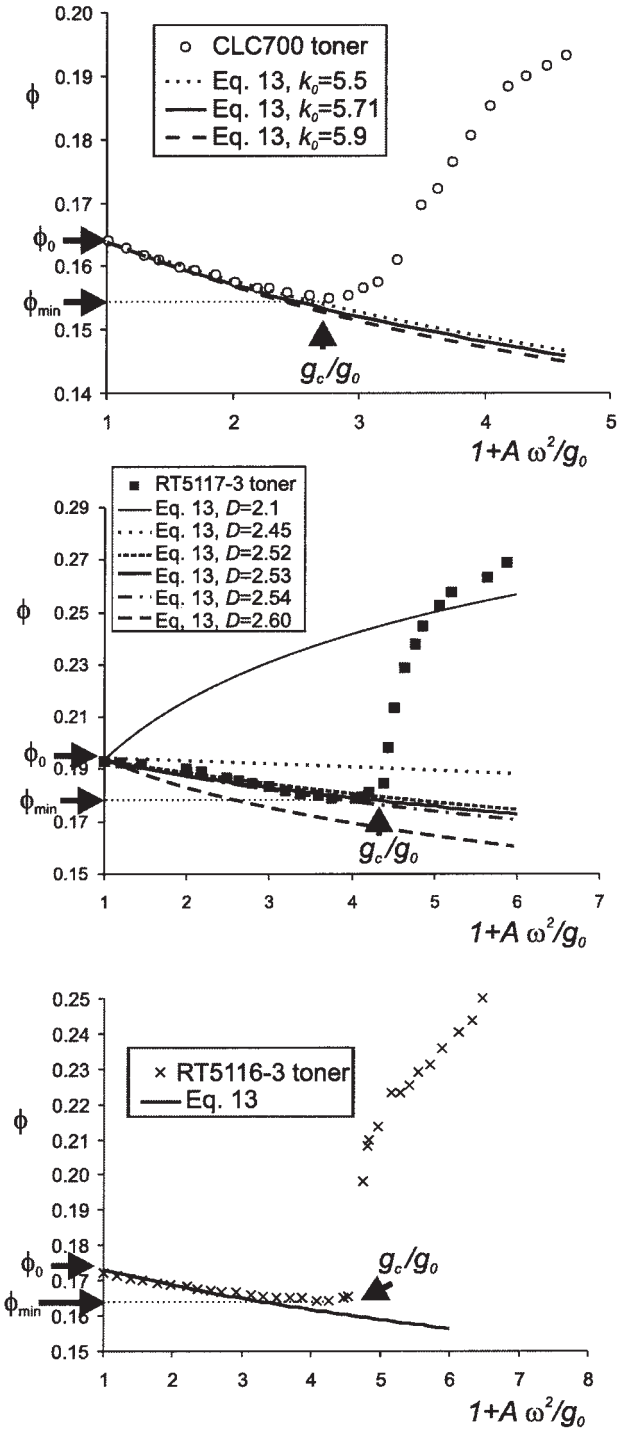

Figure 6. Particle volume fraction of the fluidized bed as the effective acceleration $g_{ef} = g_0(1 + A\omega^2/g_0)$ is increased by slowly increasing vibration amplitude at a fixed frequency $f = \omega/(2\pi)$.

The continuous curves represent the theoretical prediction by Eq. 13 for the experimental values of k_0 and D, and given in Table 1 (or otherwise indicated). CLC700 toner: $\nu_g = 0.58$ cm/s, $f = 200$ **Hz**; RT5117-3 toner: $\nu_g = 0.33$ cm/s, $f = 300$ **Hz**; RT5116-3 toner: $\nu_g = 0.33$ cm/s, $f = 300$ **Hz**.

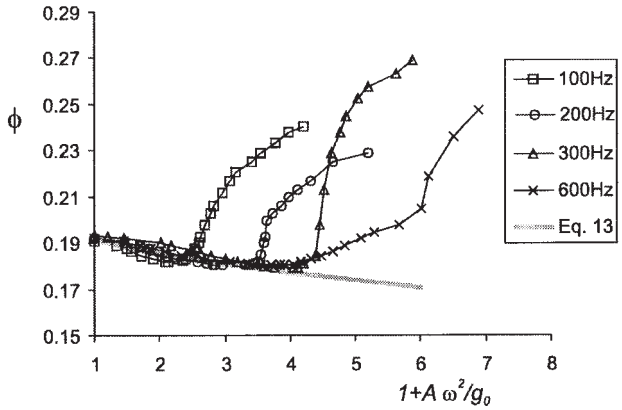

Figure 7. Particle volume fraction of the fluidized bed as the effective acceleration $g_{ef} = g_0(1 + A\omega^2/g_0)$ is increased by increasing vibration amplitude at different fixed frequencies $f = \omega/(2\pi)$ (indicated).

The continuous curve is the theoretical prediction by Eq. 13. RT5116-3 toner: $\nu_g = 0.33$ cm/s.

distribution of gas within the powder, thus, preventing uniform fluidization. We remind that according to our local state study[32] the condition of agglomerate heterogeneous fluidization (AHF) occurs for $\nu_g < 0.3$ cm/s in the case of CLC700 toner. Clearly, the dominant effect of vibration on AHF is not the size reduction of agglomerates, but the destabilization of channels and craters, thus, the bed enters progressively into an APF state of improved uniformity and enhanced expansion. In Figure 9, we have represented the minimum particle volume fraction achieved by vibration ϕ_{min} vs. the superficial gas velocity ν_g for different vibration frequencies. In accordance with our argument ϕ_{min}, for the initially AHF regime ($\nu_g < 0.3$ cm/s) is well below the theoretical prediction, whereas the measured and theoretical values are in good agreement for the initially APF regime ($\nu_g > 0.3$ cm/s).

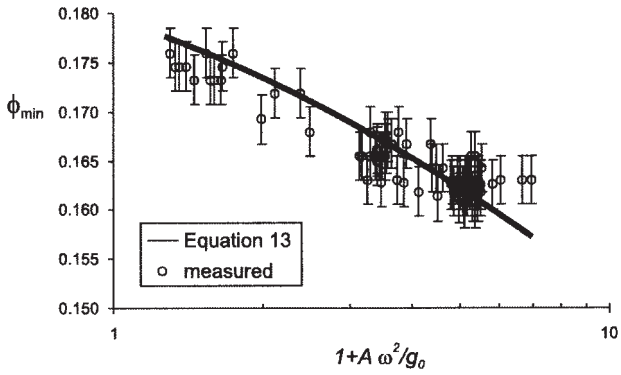

Figure 8. Particle volume fraction of a vibrofluidized bed of CLC700 toner (cm/s) just before bubbling stimulation vs. the ratio of effective acceleration to gravity acceleration at bubbling stimulation.

The predicted curve from Eq. 13 is also plotted. Each point corresponds to an experimental run performed at a given vibration frequency. Vertical error bars represent the typical indeterminacy due to bed height fluctuations.

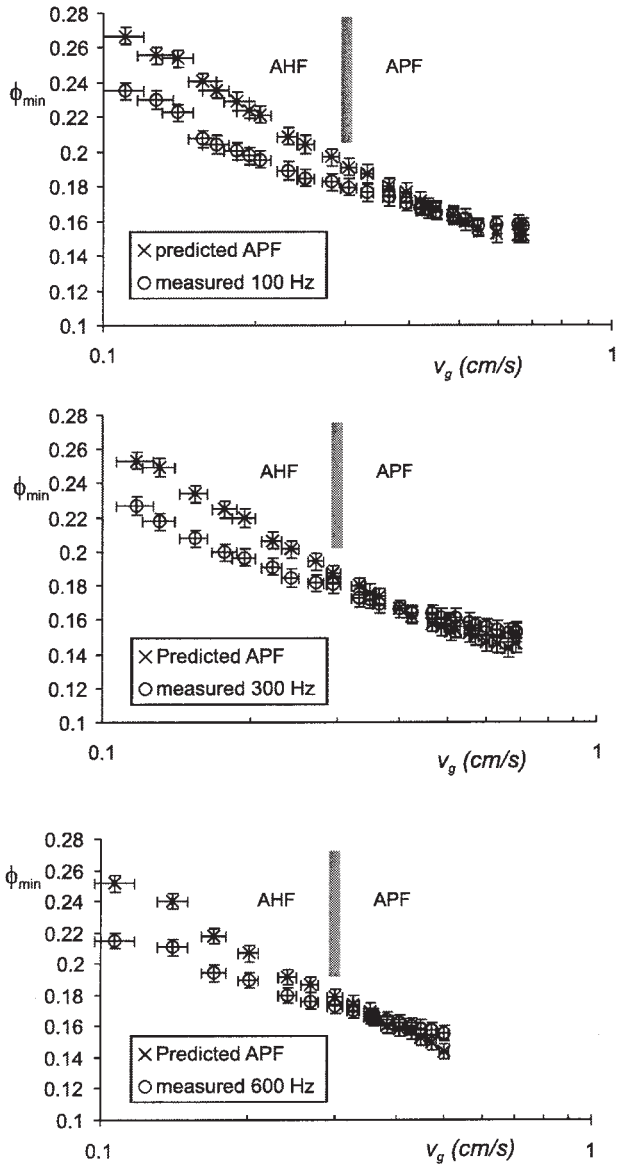

Figure 9. Particle volume fraction of the vibrofluidized bed just before bubbling stimulation as a function of the gas velocity, which is held constant during each vibration experiment.

Theoretical results are obtained from Eq. 13 using the experimental values of the critical effective acceleration. Toner CLC700. The border between AHF and APF regimes is delineated.

Let us return to the question on the physical mechanism of bubbling stimulation by vibration. We have seen that in the APF bed vibration enhances agglomerate size reduction due to the increased effective acceleration. As agglomerates become smaller and the bed expands, the agglomerate volume fraction $\phi^* = \phi k^{3-D}$ decreases. From the experimental values of ϕ and vibration amplitude at the point of bubbling stimulation we can use Eq. 12 in order to calculate the minimum value of $\phi^* = \phi^*_{min}$ (just before bubbling stimulation). In Figure 10 we have plotted ϕ^*_{min} vs. the superficial gas velocity v_g of the fluidized bed of CLC700 toner (each point corresponds to an experimental run performed at fixed frequency and gas velocity). It is seen that in the APF regime (0.3 cm/s $< v_g <$ 0.7 cm/s) ϕ^*_{min} is almost independent of v_g. Moreover, even though it decreases slightly as the vibration frequency increases, ϕ^*_{min} is close to 0.3, which is the value of $\phi^* = \phi^*_{bub}$ at incipient bubbling for the nonvibrated bed ($v_g \simeq 0.7$ cm/s, $\Lambda = 1$). Figure 11 shows the data of ϕ^*_{min} as a function of the vibration frequency for a given gas velocity ($v_g = 3.5$ mm/s). As before it is seen that ϕ^*_{min} is around $\phi^*_{bub} = 0.3$. Figure 11 also shows data of ϕ^*_{min} vs. f at fixed gas velocities in the APF regime for the Xerox toners, for which $\phi^*_{bub} \simeq 0.266$ (RT5116-3) and $\phi^*_{bub} \simeq 0.275$ (RT5117-3). As seen for the Canon toner, $\phi^*_{min} \approx \phi^*_{bub}$. We observe, however, that for low frequencies ($f \lesssim 50$ Hz) ϕ^*_{min} is systematically somewhat larger than ϕ^*_{bub}, which can be related to possible agglomerate reconstruction when $g(t) < g_0$ as discussed in the section "*Effect of Effective Acceleration on Particle Agglomeration in the APF State*".

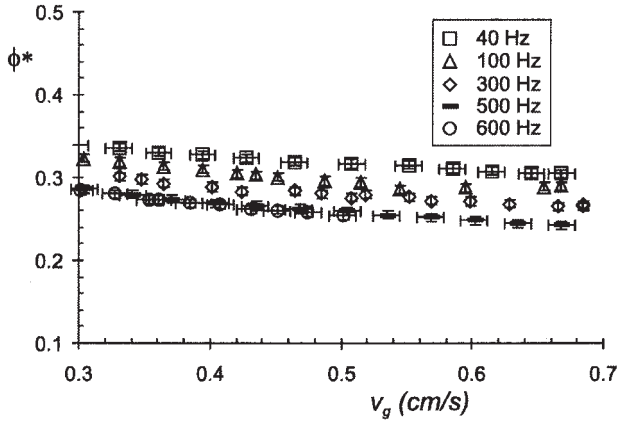

Figure 10. Agglomerate volume fraction of the vibrofluidized bed at bubbling stimulation as a function of the gas velocity, which is held constant during each vibration experiment. Data for CLC700 toner.

These results suggest that the physical mechanism of bubbling stimulation by vibration is closely related to the onset of bubbling at large gas velocities for the nonvibrated fluidized bed. In the APF bed rising local voids are rapidly split by

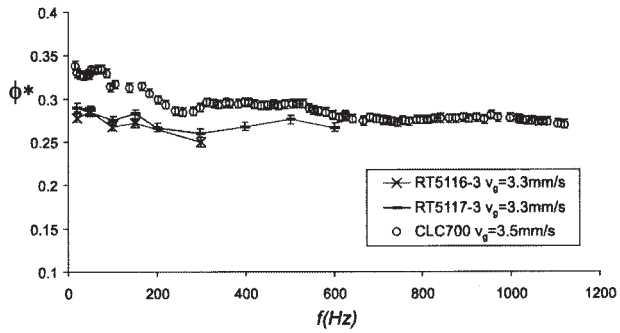

Figure 11. Agglomerate volume fraction of the vibrofluidized bed at bubbling stimulation as a function of the applied vibration frequency for a given gas velocity (indicated).

Vertical error bars represent the typical indeterminacy due to bed height fluctuations.

coherent solid pockets before being able to coalesce into large bubbles.[32] The concentration of local voids increases with gas velocity and at a critical value global bubbles are developed when the coalescence mechanism cannot be counterbalanced by void splitting. When vibration is applied to the APF bed, the induced decrease of ϕ^* and k must be accompanied by an increase of the concentration and size of the local voids. Unavoidable, there will be a critical acceleration for which their increasingly probable coalescence cannot be balanced by the splitting mechanism, resulting in the premature development of large bubbles. Bubbling stimulation has been also observed in nanoparticle fluidized beds subjected to high sound pressure level,[5] where the breakup of large agglomerate clusters takes place due to acoustic excitation. As we see in VFB, bed expansion increases monotonically as the sound pressure level increases and bubbling fluidization occurs at a certain critical value. Further increase of sound pressure yields a decrease in bed expansion, an increase in bubble frequency and an increase in bubble size in close analogy to our observations in VFB. Both phenomena might have, therefore, a similar physical origin. These results show that vibration or any other external energy source may reduce particle agglomeration, but agglomeration at some minimum level is necessary for APF.

Conclusions

In the first part of our work we have derived Eq. 13 in order to predict the expansion of a fluidized bed of fine powder in the APF regime when it is subjected to vibration while the gas velocity is held constant. This equation is based on the modified R–Z equation valid for APF (Eq. 3), and the scaling law (Eq. 8) previously derived by us on the agglomerate limit size in APF. The resulting equation has been successfully compared to experimental data on fluidized beds of xerographic toners. Vertical vibrations induce a progressive expansion of the fluidized bed as vibration amplitude is increased in agreement with our prediction. The physical mechanism responsible for bed expansion is the reduction of agglomerate size due to the increased effective gravity acceleration (Eq. 12). A side effect of the induced bed expansion and agglomerate size reduction is the increase of the concentration and size of local voids. As a consequence visible bubbles are developed and expansion is curtailed at a critical effective acceleration. According to our estimations bubbling stimulation by vibration occurs for a similar agglomerate volume fraction ϕ^*_{min} that the value $\phi^* = \phi^*_{bub}$ at incipient bubbling in the nonvibrated bed for a sufficiently large gas velocity. This coincidence suggests that the physical mechanisms for the formation of bubbles are similar in both cases. The dynamical equilibrium between splitting and coalescence of voids prevents the formation of large gas bubbles, but at the critical vibration amplitude (or gas velocity in the absence of vibration) this balance is shifted to coalescence.

Finally, it would be interesting to investigate possible resonance effects as seen by Eccles and Mujumdar on bubbling beds,[34] who observed, at the resonant point, an increase of bubble sizes of up to 215% their value in the absence of vibration. This effect occurred for relatively small vibration frequencies (0–25 Hz) and might explain our result that for low frequencies ϕ^*_{min} is larger than ϕ^*_{bub} (Figures 10 and 11). In this regime of small frequencies, for which the observed bed expansion is not significant, the effect of agglomerate shrinkage could be partially counterbalanced by agglomerate reconstruction.

Acknowledgments.

This research has been supported by Xerox Foundation and Spanish Government Agency Ministerio de Ciencia y Tecnologia (contract BFM2003-01739).

Literature Cited

1. Matsuda S, Hatano H, Tsutsumi A. Ultrafine particle fluidization and its application to photocatalytic NOx treatment. *Chem Eng J*. 2001; 82:183-188.
2. Jung J, Gidaspow D. Fluidization of nano-size particles. *J Nanopart Res*. 2002;4:483-497.
3. Yao W, Guangsheng G, Fei W, Jun W. Fluidization and agglomerate structure of nanoparticles. *Powder Technol.* 2002;124:152-159.
4. Nam CH, Pfeffer R, Dave RN, Sundaresan S. Aerated vibrofluidization of silica nanoparticles. *AIChE J*. 2004;50:1776-1785.
5. Zhu C, Liu G, Yu Q, Pfeffer R, Dave RN, Nam CH. Sound assisted fluidization of nanoparticle agglomerates. *Powder Technol*. 2004;141: 119-123.
6. Matsuda S, Hatano H, Muramoto T, Tsutsumi A. Modeling for size reduction of agglomerates in nanoparticle fluidization. *AIChE J*. 2004; 50:2763-2771.
7. Yang WC. Fluidization of fine cohesive powders and nanoparticles - A Review. *J Inst Chem Engrs*. 2005;36:1-15.
8. Zhu C, Yu Q, Dave RN, Pfeffer R. Gas fluidization characteristics of nanoparticle agglomerates. *AIChE J*. 2005;51:426-439.
9. Yu Q, Dave RN, Zhu C, Quevedo JA, Pfeffer R. Enhanced fluidization of nanoparticles in an oscillating magnetic field. *AIChE J*. 2005;51: 1971-1979.
10. Hakim LF, Portman JL, Casper MD, Weimer AW. Aggregation behaviour of nanoparticles in fluidized beds. *Powder Technol.* 2005;160: 149-160.
11. Castellanos A, Valverde JM, and Quintanilla MAS. Aggregation and sedimentation in gas-fluidized beds of cohesive powders. *Phys Rev E*. 2001;64:041304.
12. Jenneson PM, Gundogdu O. In-situ x-ray imaging of nanoparticle agglomeration in fluidized beds. *Appl Phys Lett.* 2006;88:034103(1-3).
13. Yao W, Guangsheng G, Fei W, Jun W. Fluidization and agglomerate structure of SiO2 nanoparticles. *Powder Technol*. 2002;124:152-159.
14. Valverde JM, Castellanos A, Quintanilla MAS. Effect of particle size and interparticle force on the fluidization behaviour of gas-fluidized beds. *Phys Rev E*. 2003;67:051305.
15. Richardson JF, Zaki WN. Sedimentation and fluidization: Part I. *Trans Inst Chem Engrs*. 1954;32:35-53.
16. Batchelor GK. Sedimentation in a dilute polydisperse system of interacting spheres.1. general-theory. *J Fluid Mech*. 1982;119:379-408. Batchelor GK, Wen CS. Sedimentation in a dilute polydisperse system of interacting spheres. 2. numerical results. *J Fluid Mech*. 1982;124: 495-528.
17. Valverde JM, Castellanos A. Fluidization of nanoparticles: A modified Richardson-Zaki law. *AIChE J.* 2006;52:838-842.
18. Valverde JM, Quintanilla MAS, Castellanos A, Mills P. The settling of fine cohesive powders. *Europhys Lett*. 2001;54:329-334.
19. Mawatari Y, Ikegami T, Tatemoto Y, Noda K. Prediction for Agglomerate size for fine particles in a vibro-fluidized bed. *J. Chem. Eng. Japan*. 2003;36:277-283.
20. Castellanos A, Valverde JM, Quintanilla MAS. Physics of compaction of fine cohesive powders. *Phys Rev Lett.* 2005;94:75501.
21. Kantor Y, Witten TA. Mechanical stability of tenuous objects. *J Phys Lett*. 1984;45:L675-L679.
22. Manley S, Cipelletti L, Trappe V, Bailey AE, Christianson RJ, Gasser U, Prasad V, Segre PN, Doherty MP, Sankaran S, Jankovsky AL, Shiley B, Bowen J, Eggers J, Kurta C, Lorik T, Weitz DA. Limits to gelation in colloidal aggregation. *Phys Rev Lett*. 2004;93:108302(1-3).
23. Piepers HW, Cottaar EJE, Verkooijen AHM, Rietema K. *Powder Technol*. 1984;37:55-70.
24. Valverde JM, Castellanos A. High viscosity gas fluidization of fine particles: An extended window of quasi-homogeneous flow. *Europhysics Lett*.

25. Valverde JM, Castellanos A, Ramos A, Perez AT, Morgan MA, Watson PK. An automated apparatus for measuring the tensile strength and compressibility of fine cohesive powders. *Rev Sci Instrum*. 2000; 71:2791-2795.
26. Castellanos A, Valverde JM, and Quintanilla MAS. The Sevilla Powder Tester: A tool for characterizing and investigating the physical properties of fine cohesive powders. *KONA Powder and Particle*. 2004;22:66-81.
27. Valverde JM, Castellanos A, Quintanilla MAS. Effect of vibration on the stability of a gas-fluidized bed of fine powder. *Phys Rev E*. 2001;64:021302(1-8).
28. Valverde JM, Castellanos A, Quintanilla MAS. The memory of granular materials. *Contemp Phys.* 2003;44:389-399.
29. Valverde JM, Ramos A, Castellanos A, Watson PK. The tensile strength of cohesive powders and its relationship to consolidation, free volume and cohesivity. *Powder Tech*. 1998;97:237-245.
30. Quintanilla MAS, Castellanos A, Valverde JM. Correlation between bulk stresses and interparticle contact forces in fine powders. *Phys Rev E.* 2001;64:031301(1-9).
31. Valverde JM, Castellanos A, Quintanilla MAS. Self-diffusion in a gas-fluidized bed of fine powder. *Phys Rev Lett*. 2001;86:3020-3023.
32. Valverde JM, Quintanilla MAS, Castellanos A, Mills P. Experimental study on the dynamics of gas-fluidized beds. *Phys Rev E*. 2003;67: 016303(1-5).
33. Valverde JM, Castellanos A, Quintanilla MAS. Jamming threshold of dry fine powders. *Phys Rev Lett*. 2004;92:258303(1-4).

Manuscript received Sept. 28, 2005, and revision received Dec. 9, 2005.